# Spectral Hole-Burning Studies of a Mononuclear Eu(III) Complex Reveal Narrow Optical Linewidths of the $^5D_0{\rightarrow}^7F_0$ Transition and Seconds Long Nuclear Spin Lifetimes

Sören Schlittenhardt,[a] Evgenij Vasilenko,[b, c] Vishnu Unni C.,[c] Nicholas Jobbitt,[c] Olaf Fuhr,[a, d] David Hunger,*[b, c] Mario Ruben,*[a, b, e] and Senthil Kumar Kuppusamy*[b]

Coordination complexes of rare-earth ions (REI) show optical transitions with narrow linewidths enabling the creation of coherent light-matter interfaces for quantum information processing (QIP) applications. Among the REI-based complexes, Eu(III) complexes showing the $^5D_0{\rightarrow}^7F_0$ transition are of interest for QIP applications due to the narrow linewidths associated with the transition. Herein, we report on the synthesis, structure, and optical properties of a novel Eu(III) complex and its Gd(III) analogue composed of 2,9-bis(pyrazol-1-yl)-1,10-phenanthroline (dpphen) and three nitrate ($NO_3$) ligands. The Eu(III) complex—[Eu(dpphen)($NO_3$)$_3$]—showed sensitized metal-centred emission ($^5D_0{\rightarrow}^7F_J$; J = 0,1,2,3, 4, 5, or 6) in the visible region, upon irradiation of the ligand-centred band at 369 nm, with the $^5D_0{\rightarrow}^7F_0$ transition centred at 580.9 nm. Spectral hole-burning (SHB) studies of the complex with stoichiometric Eu(III) concentration revealed a narrow homogeneous linewidth ($\Gamma_h$) of 1.55 MHz corresponding to a 0.205 μs long optical coherence lifetime ($T_{2opt}$). Remarkably, long nuclear spin lifetimes ($T_{1spin}$) of up to 41 s have been observed for the complex. The narrow optical linewidths and long $T_{1spin}$ lifetimes obtained for the Eu(III) complex showcase the utility of Eu(III) complexes as tuneable, following molecular engineering principles, coherent light-matter interfaces for QIP applications.

## Introduction

A consequence of the wavelike nature of quantum systems is their ability to produce states of superposition when adequately prepared. The superposition can be exploited for different quantum information processing (QIP) schemes, examples include quantum computation[1–4] and quantum

[a] S. Schlittenhardt, O. Fuhr, M. Ruben
Institute of Nanotechnology (INT), Karlsruhe Institute of Technology (KIT), Kaiserstraße 12, 76131, Karlsruhe, Germany
E-mail: mario.ruben@kit.edu

[b] E. Vasilenko, D. Hunger, M. Ruben, S. K. Kuppusamy
Institute of Quantum Materials and Technologies (IQMT), Karlsruhe Institute of Technology (KIT), Kaiserstraße 12, 76131, Karlsruhe, Germany
E-mail: david.hunger@kit.edu
           senthil.kuppusamy2@kit.edu

[c] E. Vasilenko, V. Unni C., N. Jobbitt, D. Hunger
Physikalisches Institut (PHI), Karlsruhe Institute of Technology (KIT), Kaiserstraße 12, 76131, Karlsruhe, Germany

[d] O. Fuhr
Karlsruhe Nano Micro Facility (KNMFi), Karlsruhe Institute of Technology (KIT), Kaiserstraße 12, 76131, Karlsruhe, Germany

[e] M. Ruben
Centre Européen de Sciences Quantiques (CESQ), Institut de Science et d'Ingénierie Supramoléculaires (ISIS), 8 allée Gaspard Monge, BP 70028, 67083 Strasbourg Cedex, France

🖳 Supporting information for this article is available on the WWW under https://doi.org/10.1002/cphc.202400280

communication.[5,6] The timescale at which a quantum mechanical system remains in the state of superposition and, therefore, the time during which QIP is possible is termed as coherence lifetime ($T_2$). Perturbations acting on the system, such as molecular vibrations[7,8] and lattice phonons,[9] amongst others, cause decoherence and reduce $T_2$. The QIP utility of different systems, such as nitrogen-vacancy centres in diamonds,[10,11] trapped ions[12,13] and rare-earth ions (REIs) doped in inorganic host lattices,[14,15] has been studied and demonstrated. Molecular complexes of trivalent REIs have been explored for QIP applications as a result of their remarkable magnetic and optical properties.[16] As their partially occupied 4f shell is well shielded from the chemical surrounding by the fully occupied 6 s and 5p shells, the interconfigurational 4f–4f transitions of REI-based complexes are narrow, translating as long optical coherence lifetimes ($T_{2opt}$). Crucially, the molecular nature of complexes allows chemical engineering of the systems, and REI-based QIP architectures with tailored physical properties can be realized.[17–19] For example, taking advantage of isotopically enriched complexes, the superposition of nuclear spin states, associated with even longer coherence times ($T_{2spin}$), can be achieved via coherent optical addressing of the 4f–4f transitions.[20–22]

The induced electric dipole $^5D_0{\rightarrow}^7F_0$ transition of Eu(III) is of particular interest for QIP, as it is only weakly influenced by magnetic perturbations and is, therefore, known to exhibit relatively long optical coherence times. The $^5D_0{\rightarrow}^7F_0$ transition is symmetry-forbidden and only observable for Eu(III) ions in low symmetry environments and is inhomogeneously broadened ($\Gamma_{inh}$) due to lattice imperfections.[23] The inhomogeneously broadened transition is composed of n-number of homoge-

**ChemPhysChem**

Research Article
doi.org/10.1002/cphc.202400280

**Chemistry Europe**
European Chemical
Societies Publishing

neously broadened transitions arising from Eu(III) centres in close energetic proximity; by estimating the homogeneous linewidth ($\Gamma_h$), $T_{2opt}$ can be determined. Spectral-hole burning (SHB) studies are used to estimate $\Gamma_h$ and $T_{2opt}$ associated with the $^5D_0 \rightarrow {}^7F_0$ transition.[24,25] Additionally, hyperfine splitting in the ground ($^7F_0$) and excited ($^5D_0$) states as well as nuclear spin lifetimes ($T_{1spin}$) can also be estimated from the SHB studies, enabling the implementation of lambda ($\lambda$)-type QIP schemes.[26]

Reports on the SHB studies of REI-based molecular complexes are scarce despite the utility of such complexes as tuneable QIP platforms. Consequently, we have recently studied three Eu(III) complexes and reported on the linewidths ($\Gamma_{inh}$ and $\Gamma_h$) and $T_{2opt}$ associated with the $^5D_0 \rightarrow {}^7F_0$ transition of the complexes.[17–19] Remarkably, long nuclear spin lifetimes ($T_{1spin}$) of the complexes have also been inferred from the SHB studies, elucidating the possibility that nuclear-spin-based qubits can be created. For one of the complexes, we have also demonstrated photon storage in the solid-state, employing atomic frequency comb (AFC) protocol, and controlled Eu(III)–Eu(III) interactions.[18] These results elucidate the potential of molecular Eu(III) complexes as optically addressable quantum materials relying on coherent light-matter interfaces with application propensity as qubits, quantum memories, and quantum gates. To progress further, it is necessary to estimate the linewidths of the $^5D_0 \rightarrow {}^7F_0$ transitions of different types of Eu(III) complexes, and the knowledge obtained from such studies can be used to shed light on factors contributing to the decoherence of the quantum superposition state. Consequently, in this contribution, we report on the linewidths ($\Gamma_{inh}$ and $\Gamma_h$), $T_{2opt}$, and $T_{1spin}$ associated with a charge-neutral mononuclear Eu(III) complex— [Eu(dpphen)(NO$_3$)$_3$]—composed of 2,9-bis(pyrazol-1-yl)-1,10-phenanthroline (dpphen) and three nitrate (NO$_3$) ligands. To determine the triplet energy ($E_T$) of the ligand, we have prepared the corresponding Gd(III) complex—[Gd-(dpphen)(NO$_3$)$_3$]. From the SHB studies, we estimate $T_{2opt} = 0.205\ \mu s$ and $T_{1spin}$ in the order of seconds at 4.2 K. These estimates obtained for the complex at stoichiometric concentration—that is, the Ln(III) positions in the crystal lattice are fully occupied by Eu(III) centres—are comparable with the ones reported for previously studied Eu(III) complexes and elucidate

the potential of molecular REI complexes as tuneable and optically addressable platforms for implementing QIP schemes.

## Results and Discussion

The aromatic system of 1,10-phenanthroline (phen) and its derivatives are known to facilitate sensitized emission of REIs, acting as a bidentate neutral antenna ligand. By tethering functional entities with metal coordination ability in the phen skeleton, the ligand's denticity can be increased.[27–30] Such tethering also modulates the electronic structure of the resultant ligand system with the consequent modulation of the optical properties. The ligand 2,9-bis(pyrazol-1-yl)-1,10-phenanthroline (dpphen) first reported by Chi *et al.*, is one such tetradentate functional phen-based ligand system.[31] Although transition metal complexes of the dpphen ligand have been studied before,[31–33] photophysical properties of the ligand and the related REI complexes are, to the best of our knowledge, yet to be studied. Taking advantage of the tetradentate nature of dpphen, we have prepared a charge-neutral Eu(III) complex —[Eu(dpphen)(NO$_3$)$_3$]—by layering a methanol solution of [Eu-(NO$_3$)$_3$·6H$_2$O] above a chloroform solution of dpphen at room-temperature (see experimental section for more details). A similar procedure was employed to prepare the Gd(III) complex —[Gd(dpphen)(NO$_3$)$_3$], as shown in Scheme 1.

Single-crystal X-ray diffraction (SC-XRD) studies revealed that complexes [Eu(dpphen)(NO$_3$)$_3$] and [Gd(dpphen)(NO$_3$)$_3$] are isostructural charge-neutral complexes. In the crystal lattice, two different variants of the [Eu(dpphen)(NO$_3$)$_3$] have been identified; the variants feature the same coordination number (CN = 10) but differ in the organization of the ligands around the Eu(III) ion. In one of the structures, the dpphen ligand occupies one meridian of the coordination sphere and the rest of the coordination sphere is occupied by three nitrate ligands, lying on the opposing meridian, each coordinating in a bidentate mode. The two pyrazole rings of the dpphen are rotated out of the plane in which the phenanthroline (phen) subunit resides, resulting in a puckered molecular structure (Figure 1, left); in the following sections this structure is referred to as [Eu(dpphen)(NO$_3$)$_3$]-puck, where puck stands for the puckered molecular structure. Among the three nitrates in
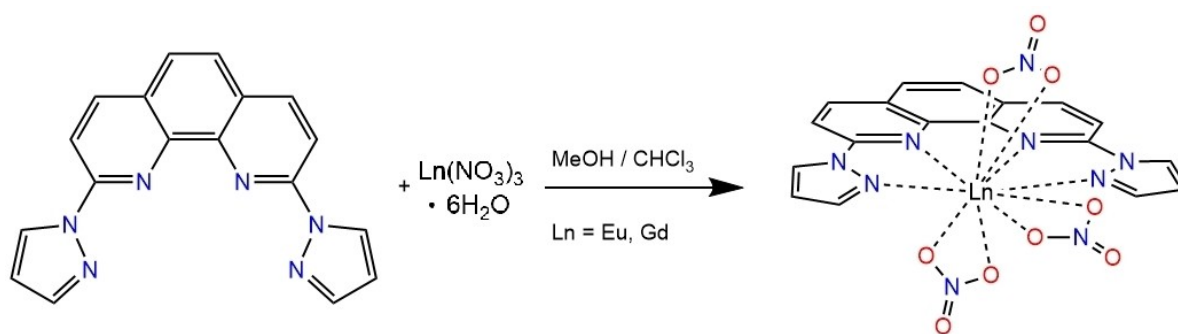


**Scheme 1.** Synthesis of [Ln(dpphen)(NO$_3$)$_3$] (Ln=Eu, Gd). The complexes are prepared by layering the lanthanide salt solution above the dpphen ligand solution. Good quality crystals suitable for structural analyses have been harvested after a few weeks.
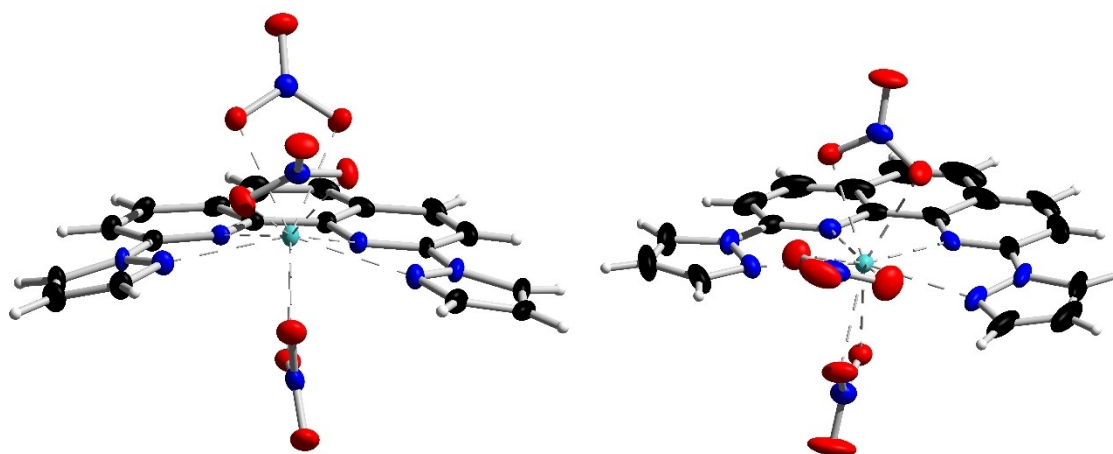
**ChemPhysChem**

Research Article
doi.org/10.1002/cphc.202400280

**Chemistry
Europe**
European Chemical
Societies Publishing

**Figure 1.** Molecular structures of the polymorphs of [Eu(dpphen)(NO$_3$)$_3$] obtained from single-crystal X-ray diffraction studies. Structures of [Eu-(dpphen)(NO$_3$)$_3$]-puck (left) and [Eu(dpphen)(NO$_3$)$_3$]-plan (right). The notations puck and plan refer to the puckered and planar organizations, respectively, of the pyrazole units of the dpphen ligand around the Eu(III) centre. Colour scheme: Eu (cyan), N (blue), O (red), C (black), H (white).

[Eu(dpphen)(NO$_3$)$_3$]-puck, one is aligning with the meridian it is located on, whereas the two remaining nitrate ligands coordinate the Eu(III) centre orthogonal with respect to their meridian. [Eu(dpphen)(NO$_3$)$_3$]-puck crystallizes in the triclinic space group $P\bar{1}$ with two molecules per unit cell and a single molecule in the asymmetric unit (Table S1). It is noted that the arrangement of the ligands results in an intrinsic chirality of the complexes; however, the crystal lattice is racemic due to the crystallization of each enantiomer in an 1 : 1 ratio.

After painstakingly probing the structures of many single crystals, we have identified a new polymorph of the Eu(III) complex crystallizing in the monoclinic space group $P2_1/c$ with four molecules per unit cell (Table S1). In the structure, the puckering of the pyrazole units is less pronounced resulting in a close to planar configuration of the dpphen ligand around the Eu(III) ion (Figure 1, right); this structure will be referred to as [Eu(dpphen)(NO$_3$)$_3$]-plan, where plan stands for planar. The coordination of the nitrate ligands in [Eu(dpphen)(NO$_3$)$_3$]-plan remains analogous to [Eu(dpphen)(NO$_3$)$_3$]-puck and the crystal lattice is racemic. The observed Eu–N distances range between 2.535(4) Å and 2.594(3) Å for [Eu(dpphen)(NO$_3$)$_3$]-puck, and 2.535(3) Å and 2.625(3) Å for [Eu(dpphen)(NO$_3$)$_3$]-plan (Table S2). The average of the Eu–N distances is 0.026 Å longer in [Eu(dpphen)(NO$_3$)$_3$]-plan than its counterpart. The elongation of the Eu–N distances in [Eu(dpphen)(NO$_3$)$_3$]-plan, compared to [Eu(dpphen)(NO$_3$)$_3$]-puck, is compensated by a reduction of the average Eu–O distances, which are found to be 0.008 Å shorter in [Eu(dpphen)(NO$_3$)$_3$]-plan than the distances observed for [Eu(dpphen)(NO$_3$)$_3$]-puck (Table S2). The Gd(III) complex also crystallized with two different polymorphs, and they are fully isostructural with the ones observed for the Eu(III) complex. In view of this point, the structural details of the Gd(III) complexes are not discussed further, see Tables S1 and S2 for structural parameters and a collection of selected bond lengths. The observation of polymorphism associated with [Ln-(dpphen)(NO$_3$)$_3$] complexes are inline with a previous report by Hasegawa and co-workers, who have also identified two differ-

ent polymorphs associated with Ln (Ln=Eu, Gd, or Tb) complexes composed of deuterated 1,10-phenanthroline and nitrate ligands.[34,35] In order to explore the coordination symmetry around the REIs, we have performed continuous shape measures (CShM)[36] analyses of the Eu(III) and Gd(III) complexes (Table S3). The coordination environment in [Ln-(dpphen)(NO$_3$)$_3$]-puck (Ln=Eu or Gd) is best described as a sphenocorona with $C_{2v}$ symmetry giving CShM values of 3.520 (Eu) and 3.453 (Gd). For the planar complexes, the coordination polyhedra is best described as a tetradecahedron with $C_{2v}$ symmetry—CShM values of 1.600 (Eu) and 1.639 (Gd) are obtained.

To estimate the ratio between the two polymorphs—[Ln(dpphen)(NO$_3$)$_3$]-x (x = puck or plan; Ln=Eu or Gd)—associated with the complexes, we have performed powder X-ray diffraction (PXRD) studies of the complexes (Figure S2). Remarkably, we have noted that the measured diffraction pattern of the bulk samples matches with the simulated patterns of [Ln(dpphen)(NO$_3$)$_3$]-puck (Ln=Eu or Gd) and no considerable reflections of [Ln(dpphen)(NO$_3$)$_3$]-plan (Ln=Eu or Gd) could be observed. Based on these observations, we conclude that bulk samples of the studied complexes are mainly composed of [Ln(dpphen)(NO$_3$)$_3$]-puck (Ln=Eu or Gd) with the planar polymorph as a minor component. However, to represent the presence of two polymorphs, we use the notation [Ln-(dpphen)(NO$_3$)$_3$] (Ln=Eu or Gd) in the following sections.

The observation of a low symmetry ($C_{2v}$) ligand-field symmetry around the Eu(III) ion in [Eu(dpphen)(NO$_3$)$_3$] encouraged us to probe the photoluminescent characteristics of the complex in the solid-state. To begin with, we have studied the PL characteristics of the dpphen ligand and [Gd(dpphen)(NO$_3$)$_3$] to determine the energies of the singlet (S$_1$) and triplet (T$_1$) excited states of the ligand. See Figures S3–S4 and the related description in the supporting information for a discussion on the S$_1$ and T$_1$ states of the dpphen ligand. The estimation of the energetic position of the T$_1$ state of the ligand ($E_T$) is important considering the fact that the energy difference between the T$_1$

state of the ligand and the Eu-based $^5D_0$ state ($\Delta E_{T1-5D0}$) is one of the factors determining the efficiency of the sensitized emission from the Eu(III)-centre, a quantity that directly influences the utility of an Eu(III)-based REI complex for QIP applications.

From the PL studies detailed in the ESI, $E_T = 20747$ cm$^{-1}$ is estimated for dpphen. Since the $E_T$ of the ligand is situated above the Eu(III)-based $^5D_0$ receiving level, Eu(III)-centred sensitized emission is expected for [Eu(dpphen)(NO$_3$)$_3$]. In line with the above point, we have observed six characteristic Eu(III)-centred $^5D_0 \rightarrow {}^7F_J$ transitions, where J = 0, 1, 2, 3, 4, 5 (Figure 2, left), upon excitation of the ligand-centred band at 369 nm (Figure S5). The highest energy $^5D_0 \rightarrow {}^7F_0$ transition is observed around 581 nm, indicating that the $^5D_0$ state is situated at 17212 cm$^{-1}$. It has been established that about 3000 cm$^{-1}$ energy difference between the triplet state of a ligand and $^5D_0$ excited state is optimal for efficient energy transfer and sensitization of Eu(III) centred emission.[19,23] In [Eu(dpphen)(NO$_3$)$_3$], the energy difference ($\Delta E_{T1-5D0}$) between the triplet state of dpphen and the $^5D_0$ state of Eu(III) is about 3535 cm$^{-1}$, which is larger than the optimal value discussed above (*vide infra*). The low intensity observed for the $^5D_0 \rightarrow {}^7F_0$ transition is in line with the symmetry forbidden nature of the transition. The relative contribution of the $^5D_0 \rightarrow {}^7F_0$ transition to the overall emission, also known as the branching ratio, is found to be 0.11%. A point noteworthy here is that the observation of the 0–0 transition confirms the low symmetry environment around the central Eu(III) inferred from the CShM analysis. The $^5D_0 \rightarrow {}^7F_J$ transitions associated with the Eu(III) complexes serve as a sensitive probe to establish spectroscopic symmetry around Eu(III) centres in a given ligand field. Since Eu(III) is a non-Kramers ion, (2 J + 1) transitions are expected for each m$_J$ state. However, the observable number of peaks depends on the ligand field symmetry around the Eu(III) centre, as discussed by Binnemans.[23] In the case of the $^5D_0 \rightarrow {}^7F_1$ transition, three peaks are expected for an Eu(III) centre in a low-symmetric

ligand field environment. A closer look into the $^5D_0 \rightarrow {}^7F_1$ transition of [Eu(dpphen)(NO$_3$)$_3$] reveals six emission peaks (Figure S6), indicating the presence of two different polymorphs of the complex in the crystal lattice. As discussed above, the Eu(III) centres in both polymorphs are placed in a ligand field environment with approximately $C_{2v}$ symmetry, justifying the observation of three peaks for each Eu-centre as a consequence of the complete lift of degeneracy associated with the $^7F_1$ state. Due to the slightly different metal-ligand interactions in each polymorph, the energetic position of the $^7F_1$ level is slightly altered causing a shift in the emission energies.

In order to estimate the lifetime ($T_{1opt}$) of the $^5D_0$ state, we have performed time-dependent emission decay studies of the Eu(III) complex at 3 K by monitoring the emission at 616 nm. By fitting the obtained decay profile with a mono-exponential function (Figure 2, right), we estimate the excited state lifetime $T_{1opt} = 1.4251 \pm 5 \times 10^{-4}$ ms. Using equations (1), (2), and (3), the radiative and non-radiative decay constants $k_{(non-)rad}$ of [Eu(dpphen)(NO$_3$)$_3$] have been estimated:

$$\tau_{rad} = \frac{I_{MD}}{A_{MD} \cdot n^3 \cdot I_{tot}} \tag{1}$$

$$k_{rad} = \frac{1}{\tau_{rad}} \tag{2}$$

$$k_{non-rad} = \frac{1}{T_{1opt}} - k_{rad} \tag{3}$$

Where $A_{MD}$ is the spontaneous emission rate of the magnetic dipole $^5D_0 \rightarrow {}^7F_1$ transition in vacuum ($A_{MD} = 14.65$ s$^{-1}$), $n$ is the refractive index of the medium and $I_{MD}/I_{tot}$ is the relative intensity of the magnetic dipole $^5D_0 \rightarrow {}^7F_1$ transition. It is a common practice in literature to approximate the refractive index of solids using the value 1.5[37–39] or 1.55.[23,40] In a recent report, Sedykh *et al.* have investigated the refractive indices of a
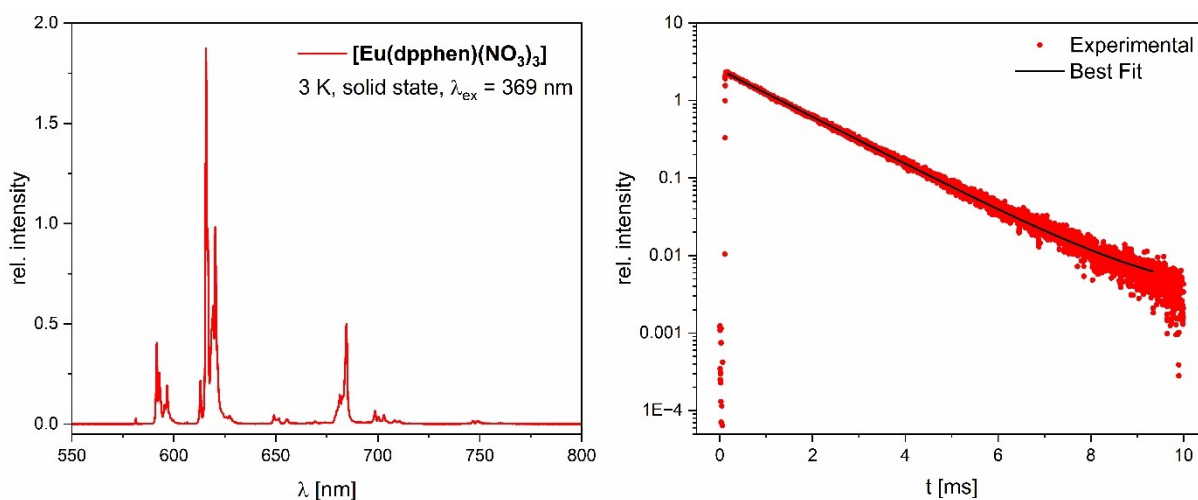


**Figure 2.** Steady-state emission spectrum (left) and luminescence decay profile (right) of [Eu(dpphen)(NO$_3$)$_3$], recorded at 3 K in the solid-state. The intensity of the PL spectrum has been normalized to the integrated intensity of the $^5D_0 \rightarrow {}^7F_1$ transition.[23] The decay profile was fitted using a mono-exponential function; An excited $^5D_0$ state lifetime ($T_{1opt}$) of $1.4251 \pm 5 \times 10^{-4}$ ms is estimated from the fit.

**ChemPhysChem**

Research Article
doi.org/10.1002/cphc.202400280

**Chemistry
Europe**
European Chemical
Societies Publishing

series of Eu(III) complexes in the solid-state using the Becke line test and have found values ranging from 1.64 to 1.71.[41] Using this information and the commonly employed approximation we have opted to assume $n = 1.65 \pm 0.1$ as a good approximation. We have found $\tau_{rad} = 2.02 \pm 0.37$ ms, $k_{rad} = 495.0 \pm 90.7$ s$^{-1}$ and $k_{non-rad} = 206.7 \pm 90.9$ s$^{-1}$. It can be seen that the radiative decay is faster than the non-radiative decay. However, $k_{non-rad}$ is not negligible, and about 29% of the excited state energy is lost via non-radiative decay, most likely facilitated by the C–H oscillators present in the dpphen ligand skeleton.

The total quantum yield ($\Phi_{tot}$) was experimentally determined at 33%. Based on the value and using equations (4) and (5), we have determined the intrinsic quantum yield ($\Phi_{Eu}$) = 71%, and with that the sensitization efficiency ($\eta_{sens}$) = 46%. As discussed previously, the determined $\Delta E_{T1-5D0} = 3535$ cm$^{-1}$ between the ligand-centred triplet state and the Eu(III)-based $^5D_0$ state is larger than the proposed optimal energy difference ($\Delta E = 3000$ cm$^{-1}$) for efficient sensitization, explaining the moderate sensitization efficiency of 46%.

$$\Phi_{Eu} = \frac{T_{1opt}}{\tau_{rad}} \qquad (4)$$

$$\Phi_{tot} = \Phi_{Eu} \, \eta_{sens} \qquad (5)$$

Photoluminescence excitation (PLE) studies of [Eu(dpphen)(NO$_3$)$_3$] at the $^5D_0 \rightarrow {^7F_0}$ transition were performed at 4.2 K by packing a polycrystalline sample of the complex in a ferrule coupled to optical fibres. Using a narrowband (< 100 kHz linewidth), tuneable dye laser, a PLE spectrum revealed a peak frequency of 17211 cm$^{-1}$ (580.916 nm) and an inhomogeneous linewidth ($\Gamma_{inh}$) of $16.44 \pm 0.03$ GHz for the $^5D_0 \rightarrow {^7F_0}$ transition of the complex (Figure 3, left). The narrow $\Gamma_{inh}$ observed for the transition is comparable with the $^5D_0 \rightarrow {^7F_0}$ linewidths reported for the previously studied Eu(III) complexes.[17–19] Importantly, the narrow $\Gamma_{inh}$ suggests high crystallinity of the [Eu(dpphen)(NO$_3$)$_3$] sample. While two polymorphs have been observed crystallographically as well as spectroscopically, only a single line was observed for the $^5D_0 \rightarrow {^7F_0}$ transition of [Eu(dpphen)(NO$_3$)$_3$] in the PLE studies. We associate the single-line to the [Eu(dpphen)(NO$_3$)$_3$]-puck poly-

morph as it is the dominant species in the crystal lattice (see the discussion above).

Spectral hole-burning (SHB) was performed by applying a laser pump pulse of 500 ms duration at a fixed frequency. This redistributes the hyperfine population through optical excitation and relaxation. Subsequently, a PLE spectrum is taken around the pump frequency, employing a probe pulse of 200 ms duration where the frequency was swept over 60 MHz, which probes the prepared spectral hole. By estimating the hole width ($\Gamma_{hole}$), the homogeneous linewidth ($\Gamma_h$) can be derived, which in turn can be used to estimate the $T_{2opt}$, employing equation 6.

$$\Gamma_h = \frac{1}{\pi \cdot T_{2opt}} \qquad (6)$$

From the SHB studies, we have estimated a hole-width of $3.10 \pm 0.31$ MHz, corresponding to $\Gamma_h = 1.55 \pm 0.16$ MHz and $T_{2opt} = 205 \pm 21$ ns for [Eu(dpphen)(NO$_3$)$_3$].

After hole-burning, nuclear spins are depopulated from one set of ground-state hyperfine (HF) levels. With time, the spins relax and the equilibrium population in the ground state HF states is restored. This implies that time-dependent studies of hole-depth after the burning sequence would shed light on the nuclear spin lifetimes ($T_{1spin}$). Estimation of $T_{1spin}$ is important as it provides an upper time limit for $T_{2spin}$, which is the timescale available for creating coherent superposition between HF levels. Consequently, we have monitored the time-dependent evolution of the hole-depth to estimate $T_{1spin}$ (Figure 4). The time versus hole-depth data depicted in Figure 4 can be fitted with a biexponential decay, yielding two time constants $T_{1spin\ (short)} = 0.31 \pm 0.14$ s and $T_{1spin\ (long)} = 41.39 \pm 5.29$ s. The observed biexponential decay of the hole-width of [Eu(dpphen)(NO$_3$)$_3$] is consistent with similar decays observed for the previously studied Eu(III) complexes.[17–19] The origin of the two distinct relaxation time regime in molecular Eu(III) complexes is not fully understood. We tentatively attribute such relaxation process to different time constants associated with different HF states involved and with different relaxation mechanisms—examples include Orbach and Raman processes—causing spin-relaxation.[42]
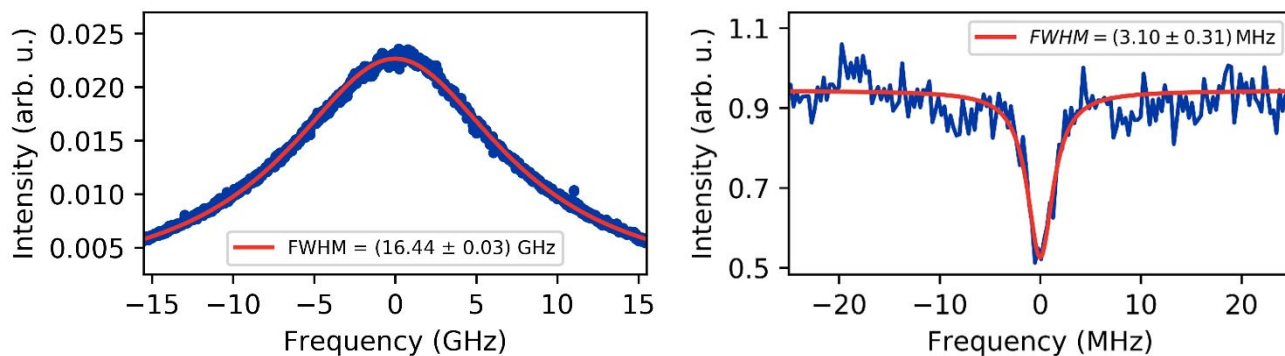


**Figure 3.** SHB studies of [Eu(dpphen)(NO$_3$)$_3$]. Inhomogeneously broadened line measured (left) and spectral hole (right) observed for [Eu(dpphen)(NO$_3$)$_3$] after applying a spectral burning pulse sequence. All measurements were recorded on a solid sample at 4.2 K. In both plots the red lines correspond to the best fit employing a Lorentzian profile.
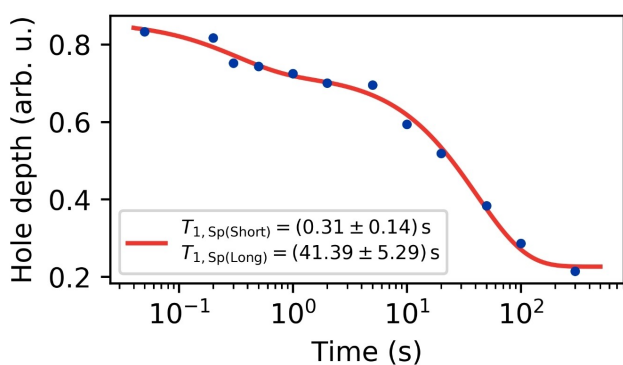
**ChemPhysChem**

Research Article
doi.org/10.1002/cphc.202400280

**Chemistry
Europe**
European Chemical
Societies Publishing

**Figure 4.** Plot of the experimentally determined hole depth after applying the spectral hole burning sequence against increasing waiting times between the burning and measuring pulse. The data was recorded at 4.2 K and the red line indicates the best fit to a biexponential decay.

In the foregoing sections, we have discussed the steady-state and time-dependent photoluminescent characteristics of [Eu(dpphen)(NO$_3$)$_3$]. We have shed light on the homogeneous and inhomogeneous linewidths and nuclear spin lifetimes associated with the complex by performing SHB studies. A notable feature is the 1.4251 ms excited state lifetime estimated for the [Eu(dpphen)(NO$_3$)$_3$], setting a lower-limit of 112 Hz for the homogeneous linewidth. However, the estimated $\Gamma_h$ (1.55 MHz) for the complex is much larger than the lifetime-limited linewidth, indicating the presence of other broadening mechanisms such as spectral-diffusion, in line with the reports dealing with Eu(III) centres doped in host lattices.[42,43] The $\Gamma_{inh}$ and $\Gamma_h$ estimated for [Eu(dpphen)(NO$_3$)$_3$] are in the range reported for the previously studied Eu(III) complexes, elucidating the fact that narrow linewidths of the $^5D_0 \rightarrow {}^7F_0$ transition are an intrinsic property of molecular Eu(III) complexes.

The appeal of molecular, Eu(III)-based complexes stems from the tuneable nature of their photophysical properties following molecular engineering priciples, a possibility not readily accesible with REI-doped host lattices, as demonstrated for four complexes, including the one discussed in this study. Furthermore, the low symmetry coordination environment of the central ion in molecular complexes enhances the oscillator strength of the $^5D_0 \rightarrow {}^7F_0$ transition. An increased oscillator strength is essential to facilitate single ion detection and control. Further, this can allow ensemble quantum memories with better efficiency. For a detailed discussion on various parameters governing the emission characteristics of molecular Eu(III) complexes, the reader is advised to refer to a previous report from our side[19] and a biblical review from K. Binnemans.[23] In the following section, we provide a comparative description of the inhomogeneous and homogeneous linewidths associated with Eu(III) centres doped in host lattices and stoichiometric Eu(III) systems that include EuCl$_3$·6H$_2$O,[44] EuP$_5$O$_4$,[45] and molecular REI complexes.[17–19]

Concentration-dependent inhomogeneous linewidths have been reported for Eu(III) centres doped in host lattices. For Eu(III):Y$_2$SiO$_5$, inhomogeneous linewidths of 0.5 GHz and 150 GHz were estimated at 0.02% and 7% Eu(III) concentra-

tions, respectively.[42] The increase in linewidth with increasing Eu(III) concentration in Eu(III):Y$_2$SiO$_5$ is attributed to strain induced by the ionic radii mismatch between the Eu(III) and Y(III) centres. In the case of stoichiometric systems, Eu(III) is the only REI present in the lattice, ruling out ionic radii differences as a factor causing inhomogeneous linebroadening. Consequently, we relate the inhomogeneous linewidths associated with the stoichiometric systems to the crystalline quality. For a single-crystal of EuCl$_3$·6H$_2$O, an inhomogeneous linewidth of 600 MHz is observed for the structured line associated with the $^5D_0 \rightarrow {}^7F_0$ transition. The linewidth of the structured transition can be further narrowed by isotopically enriching the system with $^{35}$Cl and its hyperfine structure can be resolved with each hyperfine line featuring around 25 MHz of inhomogeneous broadening.[44] In the case of EuP$_5$O$_4$, an inhomogeneous linewidth of 3.5 GHz was estimated.[45] Remarkably, the linewidth is asymmetric and a position dependence was observed. This indicates inhomogeneities associated with the crystal lattice of EuP$_5$O$_4$. The inhomogeneous linewidths observed for the Eu(III)-based molecular complexes are larger than the widths observed for Eu(III) centres doped into inorganic host lattices at a concentration of about 0.02% and those of a stoichiometric single-crystal of EuCl$_3$·6H$_2$O. On the other hand, the linewidths estimated for the molecular Eu(III)-based complexes are in the GHz regime as observed for EuP$_5$O$_4$. In the case of molecular systems, polycrystalline samples are used due to the small size of the crystals. The polycrystalline nature and poor quality of the molecular crystals could have caused linebroadening, an assumption agreeing well with the observations made for EuP$_5$O$_4$. The above discussion relating broad inhomogeneous linewidths with crystalline quality indicates that in crystals of high-quality it is possible to resolve hyperfine transitions, as in the case of EuCl$_3$·6H$_2$O, and isotopic enrichment can be leveraged to obtain narrow inhomogeneous linewidths associated with hyperfine transitions, see the discussion by R. M. Macfarlane.[43] The inhomogeneous linewidths observed for rare-earth complexes clearly indicate that their crystal lattices are highly strained and isotopic enrichment is of little importance. Consequently, to obtain narrow linewidths it is necessary to grow large and high-quality single-crystals of REI complexes. In the specific example of [Eu(dpphen)(NO$_3$)$_3$], two-photon absorption at 581 nm of the organic antenna and the presence of two different molecular structures inherently leading to disorder due to different packing modes of the structures would have contributed to the line broadening. The inhomogeneous linewidth is a highly relevant metric in terms of QIP application. An inhomogeneous linewidth more narrow than the hyperfine splitting could open up interesting possibilities, as it enables direct addressing and readout of the HF levels without prior optical pumping. Depending on the QIP protocol, however, both narrow and wide inhomogeneous lines can be desirable.[46] For example, the CRIB (controlled reversible inhomogeneous broadening) protocol requires narrow inhomogeneous linewidths, while the AFC (atomic frequency comb) protocol benefits from broad inhomogeneous lines for the realization of efficient quantum memories.[47] The point here is disorder is not bad when system bandwidth is considered.

The homogeneous linewidth of 1.55 MHz observed for [Eu(dpphen)(NO$_3$)$_3$] is comparable with the values reported for previously studied Eu(III)-based complexes. A direct comparison between the homogeneous linewidth estimated for the REI-doped and molecular systems is rendered difficult due to the use of photon echo (PE) and SHB techniques, respectively, used determine the width. The widths obtained from the SHB studies are always broader than the ones obtained from PE studies, as exemplified for a mononuclear Eu(III) complex—[Eu(BA)$_4$][(pip)], where BA and pip stand for the anionic benzoylacetonate ligand and piperidinium cation, respectively.[18] However, a point noteworthy here is homogeneous linewidths close to lifetime-limited ones have been measured for REI-doped crystals—for example, Er$^{3+}$:Y$_2$SiO$_5$ ($\Gamma_h = 50$ Hz) and Eu$^{3+}$:Y$_2$O$_3$ ($\Gamma_h = \sim100$ Hz).[48,49] Close to lifetime limited linewidth has also been reported for the stoichiometric EuCl$_3$·6D$_2$O ($\Gamma_h = 430$ Hz).[50] The above points elucidate that homogeneous linewidths obtained for the molecular systems are about six orders larger than the ones obtained for Eu$^{3+}$:Y$_2$O$_3$ and stoichiometric EuCl$_3$·6D$_2$O. In the case of EuCl$_3$·6D$_2$O, replacing deuterium with hydrogen led to the broadening of the linewidth by about an order—for EuCl$_3$·6H$_2$O, $\Gamma_h = 4.1$ kHz is reported.[50] Such broadening indicates the role of nuclear spin bearing isotopes in increasing the homogeneous linewidth. In a previous study concerning [Eu(BA)$_4$][(pip)], it was demonstrated that two-level systems created by low-frequency vibrational modes and spectral diffusion contribute to the homogeneous linebroadening. By taking a leaf from the above discussion, the observed homogeneous linebroadening in [Eu(dpphen)(NO$_3$)$_3$] is attributed to mechanisms such as nuclear-spin bath, spin–phonon interactions, and spectral diffusion.

The knowledge on the inhomogeneous and homogeneous linewidths associated with [Eu(dpphen)(NO$_3$)$_3$] allows for a comparison between the QIP metrics of the so far studied molecular rare-earth systems. As discussed before, a broad inhomogeneous linewidth is advantageous for frequency multiplexing. The number of available frequency modes (N$_f$) available for storage within an inhomogeneously broadened line can be calculated using equation 7 proposed by Ortu et al.[47]

$$N_f = \Gamma_{inh}/2(\Delta g + \Delta e) + \Delta f \qquad (7)$$

In equation 7, $\Delta g$ and $\Delta e$ are the frequency separations between the ground and excited hyperfine states, respectively, and $\Delta f$ is the width of the absorption teeth in a frequency comb. In the absence of direct measurements for [Eu(dpphen)(NO$_3$)$_3$], we have used $\Delta g + \Delta e = 139.6$ MHz and $\Delta f = 0.9$ MHz obtained for [Eu(BA)$_4$][(pip)]. Using equation (7), N$_f = 58$ is calculated for [Eu(dpphen)(NO$_3$)$_3$], the value is comparable with the ones obtained for previously studied molecular systems—[Eu(BA)$_4$](pip) (N$_f = 24$), [Eu(trensal)] (N$_f = 325$), where trensal stands for 2,2′,2″-tris(salicylideneimino)triethylamine, and [Eu$_2$] (N$_f = 179$), where [Eu$_2$] is a bimetallic Eu(III) complex with six chloride and six 4-picoline N- oxide ligands.[17–19]

Optical coherence lifetime and nuclear spin lifetimes are two other important QIP metrics estimated for [Eu(dpphen)(NO$_3$)$_3$] from the SHB studies. A comparison of the $T_{2opt}$ values obtained for the Eu(III) complexes studied so far results in the following order: [Eu(BA)$_4$](pip) (370 ns) > [Eu(dpphen)(NO$_3$)$_3$] (205 ns) > [Eu(trensal)] (114 ns) > [Eu$_2$] (14.5 ns). Note, all values are from SHB studies. The determined nuclear spin lifetime of up to 41 s for [Eu(dpphen)(NO$_3$)$_3$] is also in the range reported for molecular Eu(III) systems. These points emphasize the fact that molecular complexes feature remarkable $T_{2opt}$ and $T_{1spin}$ even at stoichiometric concentrations and are suitable for implementing QIP protocols.

## Conclusions

Two Ln(III) complexes—[Eu(dpphen)(NO$_3$)$_3$] and [Gd-(dpphen)(NO$_3$)$_3$]—composed of a central REI, dpphen and nitrate ligands have been prepared and their molecular structures have been elucidated by performing SC-XRD studies. In the crystalline samples of each Ln(III) complex, there are two distinct crystallographic polymorphs with slightly different coordination environments. Each polymorph differs from the other based on how the dpphen ligand is organized around the Ln(III) centre. In the dominant polymorph—[Ln(dpphen)(NO$_3$)$_3$]-puck—the coordinating pyrazole units are rotated in opposite directions and the Ln(III) ion sits above the phen-plane. In the case of the minor polymorph—[Ln(dpphen)(NO$_3$)$_3$]-plan—the metal ion lies inside the phen-plane and the pyrazole rings are rotated in the same direction. The Eu(III) complex shows bright sensitized emission upon excitation in the UV region, revealing the presence of the $^5D_0 \rightarrow ^7F_0$ transition, which can possibly be exploited for QIP schemes considering the narrow linewidth associated with the transition. From the SHB studies of the stoichiometric crystals of [Eu(dpphen)(NO$_3$)$_3$], we have estimated narrow inhomogeneous and homogeneous linewidths of 16.44 GHz and 1.55 MHz, respectively, and an optical coherence lifetime of 205 ns. The observed nuclear spin lifetime of the complex is in the order of seconds, elucidating the possibility that hyperfine qubits can be realized. Overall, the results presented in this study indicate the promise of molecular Eu(III) complexes as coherent light-matter interfaces with QIP application propensity.

## Experimental Section

All starting materials were received from commercially available sources and used without further purification. The ligand dpphen was synthesized following a previously reported procedure.[32]

Preparation of [Ln(dpphen)(NO$_3$)$_3$] (Ln=Eu, Gd) complexes: The complexes were prepared by layering a methanolic solution (10 ml) of [Ln(NO$_3$)$_3$·6H$_2$O] (0.1 mmol, 1 eq., 44.6 mg (Ln=Eu); 45.1 mg (Ln=Gd)) above a 20 ml solution of dpphen (0.1 mmol, 1 eq., 32.0 mg) in chloroform and the two phase mixture was allowed to stand at RT. After several hours, crystals of the complexes started to appear at the interface, and the mixture was allowed to stand for two weeks. After that, the crystals were collected by decanting off the mother liquor and washing them twice with chloroform and methanol to remove any unreacted starting material. The complexes were obtained as colourless block-shaped crystals.

[Eu(dpphen)(NO$_3$)$_3$]:

Yield: 53.3 mg, (82%). Elemental analysis: Calculated for C$_{18}$H$_{12}$EuN$_9$O$_9$: C, 33.25%; H, 1.86%; N, 19.39%. Found: C, 32.68%; H, 1.76%; N, 19.28%., ATR-IR: see Figure S1.

[Gd(dpphen)(NO$_3$)$_3$]:

Yield: 50.5 mg, (77%). Elemental analysis: Calculated for C$_{18}$H$_{12}$GdN$_9$O$_9$: C, 32.98%; H, 1.85%; N, 19.23%. Found: C, 34.70%; H, 2.16%; N, 19.22%., ATR-IR: see Figure S1.

### Single-Crystal X-ray Diffraction Studies

The studies were performed using a "STOE" IPDS 2T diffractometer with an image plate detector and Mo-K$_\alpha$ radiation. The crystals were placed in a cold nitrogen stream (180 K) during data collection. Data reduction was performed using the CrysAlisPro software package[51] and the structures were solved and refined using SHELXL[52] implemented into Olex2.[53] All non-hydrogen atoms were refined anisotropically and hydrogens were placed following a riding model.

### Powder X-ray Diffraction Studies

Powder diffraction patterns were collected on a "STOE" Stadi P diffractometer at room temperature using Cu–Kα radiation. Simulated P-XRD patterns were obtained using SC-XRD data using Mercury[54].

### Steady-State and Time-Resolved PL Studies

PL measurements at cryogenic and room temperature were performed on a "Horiba" Fluorolog spectrometer with a 920 photomultiplier tube detector. The powdered samples were placed in between two quartz glass plates with a drop of perfluorinated oil. A 400 nm long pass filter was used to cut the second- and higher-order diffraction peaks in the spectra. Quantum yields were determined at room temperature using a QuantaPhi-2 Integrating sphere with an internal diameter of 121 mm.

### Spectral-Hole Burning Studies

Investigation of the inhomogeneous linewidth and spectral hole burning measurements were performed by placing the powdered sample in a copper ferrule connected to a multimode fibre with a 200 μm core diameter. The ferrules were placed in a home-built dipstick cryostat, which was fully evacuated and subsequently filled with a small amount of He exchange gas to allow better thermalization. The dipstick was placed in liquid helium to reach 4.2 K. A Sirah Matisse 2 DX dye laser with a linewidth < 100 kHz was used as excitation source.

## Supporting Information Summary

Additional supporting information can be found online in the Supporting Information section at the end of this article.

## Conflict of Interests

The authors declare no conflict of interest.

## Data Availability Statement

Deposition Number(s) 2333091 (for [Eu(dpphen)(NO$_3$)$_3$]-puck), 2333092 (for [Gd(dpphen)(NO$_3$)$_3$]-puck), 2333093 (for [Eu-(dpphen)(NO$_3$)$_3$]-plan), 2333095 (for [Gd(dpphen)(NO$_3$)$_3$]-plan), contain(s) the supplementary crystallographic data for this paper. These data are provided free of charge by the joint Cambridge Crystallographic Data Centre and Fachinformationszentrum Karlsruhe Access Structures service.

All the remaining data presented in the manuscript are available either in the main script or supporting information.

[1] M. Brooks, *Nature* **2023**, *617*, S1–S3.
[2] F. de Lima Marquenzino, R. Portugal, C. Lavor, *A Primer on Quantum Computing*, Springer, Cham, Switzerland **2019**.
[3] C. Godfrin, A. Ferhat, R. Ballou, S. Klyatskaya, M. Ruben, W. Wernsdorfer, F. Balestro, *Phys. Rev. Lett.* **2017**, *119*, 187702.
[4] Y.-X. Wang, Z. Liu, Y.-H. Fang, S. Zhou, S.-D. Jiang, S. Gao, *Npj. Quantum Inf.* **2021**, *7*, 32.
[5] N. Gisin, R. Thew, *Nat. Photon* **2007**, *1*, 165–171.
[6] J. Chen, *J. Phys.: Conf. Ser.* **2021**, *1865*, 022008.
[7] N. P. Kazmierczak, R. Mirzoyan, R. G. Hadt, *J. Am. Chem. Soc.* **2021**, *143*, 17305–17315.
[8] S. Mondal, A. Lunghi, *Npj. Comput. Mater.* **2023**, *9*, 120.
[9] V. Kornich, M. G. Vavilov, M. Friesen, S. N. Coppersmith, *New J. Phys.* **2018**, *20*, 103048.
[10] L. Childress, R. Hanson, *MRS Bull.* **2013**, *38*(2), 134–138.
[11] M. W. Doherty, N. B. Manson, P. Delaney, F. Jelezko, J. Wrachtrup, L. C. L. Hollenberg, *Phys. Rep.* **2019**, *528*, 1–45.
[12] J. I. Cirac, P. Zoller, *Phys. Rev. Lett.* **1995**, *74*, 4091–4094.
[13] C. D. Bruzewicz, J. Chiaverini, R. McConnell, J. M. Sage, *Appl. Phys. Rev.* **2019**, *6*, 021314.
[14] R. Giraud, W. Wernsdorfer, A. M. Tkachuk, D. Mailly, B. Barbara, *Phys. Rev. Lett.* **2001**, *87*, 057203.
[15] S. Bertaina, S. Gambarelli, A. Tkachuk, I. N. Kurkin, B. Malkin, A. Stephanov, B. Barbara, *Nat. Nanotech.* **2007**, *2*, 39–42.
[16] R. Marin, G. Brunet, M. Murugesu, *Angew. Chem. Int. Ed.* **2021**, *60*, 1728–1746.
[17] S. K. Kuppusamy, D. Serrano, A. M. Nonat, B. Heinrich, L. Karmazin, L. Charbonniere, P. Goldner, M. Ruben, *Nat. Commun.* **2021**, *12*, 2152.
[18] D. Serrano, S. K. Kuppusamy, B. Heinrich, O. Fuhr, D. Hunger, M. Ruben, P. Goldner, *Nature* **2022**, *603*, 241–246.
[19] S. K. Kuppusmay, E. Vasilenko, W. Li, J. Hessenauer, C. Ioannou, O. Fuhr, D. Hunger, M. Ruben, *J. Phys. Chem. C* **2023**, *127*, 10670–10679.

[20] C. J. Ballance, T. P. Harty, N. M. Linke, M. A. Sepiol, D. M. Lucas, *Phys. Rev. Lett.* **2016**, *117*, 060504.

[21] J. J. Pla, K. Y. Tan, J. P. Dehollain, W. H. Lim, J. J. L. Morton, F. A. Zwanenburg, D. N. Jamieson, A. S. Dzurak, A. Morelllo, *Nature* **2013**, *496*, 334–338.

[22] S. Thiele, F. Balestro, R. Ballou, S. Klyatskaya, M. Ruben, W. Wernsdorfer, *Science* **2014**, *344*, 1135–1138.

[23] K. Binnemans, *Coord. Chem. Rev.* **2015**, *295*, 1–45.

[24] W. E. Moerner, *Persistent Spectral Hole-Burning*, Springer, Heidelberg, Germany **2012**.

[25] C. H. Brito Cruz, J. P. Gordon, P. C. Becker, R. L. Fork, C. V. Shank, *IEEE J. Quantum Electron.* **1988**, *24*, 261–269.

[26] P. Goldner, A. Ferrier, O. Guillot-Noël, in *Handbook on the Physics and Chemistry of Rare Earths: Chapter 267: Rare Earth-Doped Crystals for Quantum Information Processing* (Eds: J.-C. G. Bünzli, V. K. Pecharsky), Elsevier, Amsterdam **2015**, 1–78.

[27] R. Ziessel, *Tetrahedron Lett.* **1989**, *30*(4), 463–466.

[28] G. G. Zakirova, D. Y. Mladentsev, N. E. Borisova, *Tetrahedron Lett.* **2017**, *58*(35), 3415–3417.

[29] N. E. Borisova, A. V. Kharcheva, S. V. Patsaeva, L. A. Korotkov, S. Bakaev, M. D. Reshetova, K. A. Lyssenko, E. V. Belova, B. F. Myasoedov, *Dalton Trans.* **2017**, *46*, 2238–2248.

[30] L. Xu, X. Yang, Z. Wang, S. Wang, M. Sun, C. Xu, X. Zhang, L. Lei, C. Xiao, *Inorg. Chem.* **2021**, *60*(4), 2805–2815.

[31] Y.-H. Chi, W. Wie, J.-M. Shi, Y.-Q. Zhang, S.-L. Liu, *J. Coord. Chem.* **2012**, *65*(13), 2378–2390.

[32] G.-L. Li, S.-Q. Wu, L.-F. Zhang, Z. Wang, Z.-W. Ouyang, Z.-H. Ni, S.-Q. Su, Z.-S. Yao, J.-Q. Li, O. Sato, *Inorg. Chem.* **2017**, *56*, 8018–8025.

[33] J.-Y. Li, Y.-L. Huang, T.-C. Li, Y. Li, L.-X. Wang, L. Zhang, X. Zhang, J. Xiang, *Z. Anorg. Allg. Chem.* **2023**, *649*, e202300138.

[34] F. Werner, K. Tada, A. Ishii, M. Takata, M. Hasegawa, *CrystEngComm* **2009**, *11*, 1197–1200.

[35] S. Ogata, A. Ishii, C. L. Lu, T. Kondo, N. Yajima, M. Hasegawa, *J. Photochem. Photobiol., A* **2017**, *334*, 55–60.

[36] M. Pinsky, D. Avnir, *Inorg. Chem.* **1998**, *37*(21), 5575–5582.

[37] J.-C. G. Bünzli, A.-S. Chauvin, H. K. Kim, E. Deiters, S. V. Eliseeva, *Coord. Chem. Rev.* **2010**, *254*, 2623–2633.

[38] S. V. Eliseeva, D. N. Pleshkov, K. A. Lyssenko, L. S. Lepnev, J.-C. G. Bünzli, N. P. Kuzmina, *Inorg. Chem.* **2011**, *50*, 5137–5144.

[39] Y. Hasegawa, S. Natori, J. Fukudome, T. Nagase, T. Kobayashi, T. Nakanishi, Y. Kitagawa, K. Fushimi, H. Naito, *J. Phys. Chem. C.* **2018**, *122*, 9599–9605.

[40] O. T. Alexander, R. E. Kroon, A. Brink, H. G. Visser, *Dalton Trans.* **2019**, *48*, 16074–16082.

[41] A. E. Sedykh, M. Maxeiner, M. T. Seuffert, D. Heuler, D. G. Kurth, K. Müller-Buschbaum, *Eur. J. Inorg. Chem.* **2024**, e202400078.

[42] F. Könz, Y. Sun, C. W. Thiel, R. L. Cone, R. W. Equall, R. L. Hutcheson, R. M. Macfarlane, *Phys. Rev. B* **2003**, *68*, 085109.

[43] R. M. Macfarlane, *J. Lumin.* **2002**, *100*, 1–20.

[44] R. L. Ahlefeldt, M. R. Hush, M. J. Sellars, *Phys. Rev. Lett.* **2016**, *117*, 250504.

[45] R. M. Shelby, R. M. Macfarlane, *Phys. Rev. Lett.* **1980**, *45*, 1098–1101.

[46] C. W. Thiel, T. Böttger, R. L. Cone, *J. Lumin.* **2011**, *131*, 353–361.

[47] A. Ortu, J. V. Rakonjac, A. Holzäpfel, A. Seri, S. Grandi, M. Mazzera, H. de Riedmatten, M. Afzelius, *Quantum Sci. Technol.* **2022**, *7*, 035024.

[48] Y. Sun, C. W. Thiel, R. L. Cone, R. W. Equall, R. L. Hutcheson, *J. Lumin.* **2002**, *98*, 281–287.

[49] R. W. Equall, Y. Sun, R. L. Cone, R. M. Macfarlane, *Phys. Rev. Lett.* **1994**, *72*, 2179–2182.

[50] R. L. Ahlefeldt, N. B. Manson, M. J. Sellars, *J. Lumin.* **2003**, *133*, 152–156.

[51] Agilent, CrysAlis PRO, Agilent Technologies Ltd, Yarnton, Oxfordshire, England **2014**.

[52] G. M. Sheldrick, *Acta Cryst. C* **2015**, *71*, 3–8.

[53] O. V. Dolomanov, L. J. Bourhis, R. J. Gildea, J. A. K. Howard, H. Puschmann, *J. Appl. Cryst.* **2009**, *42*, 339–341.

[54] C. F. Macrae, P. R. Edgington, P. McCabe, E. Pidcock, G. P. Shields, R. Taylor, M. Towler, J. van de Streek, *J. Appl. Cryst.* **2006**, *39*, 453–457.